ELSEVIER

Ceramics International 28 (2002) 79–91

CERAMICS INTERNATIONAL

www.elsevier.com/locate/ceramint

Mechanical and thermal behaviour of cordierite–zirconia composites

F.A. Costa Oliveira[a,*], J. Cruz Fernandes[b]

[a]*Instituto Nacional de Engenharia e Tecnologia Industrial, Departamento de Materiais e Tecnologias de Produção, Estrada do Paço do Lumiar, 1649-038 Lisbon, Portugal*

[b]*Instituto Superior Técnico, Departamento de Engenharia de Materiais, Av. Rovisco Pais, 1049-001 Lisbon, Portugal*

Received 14 November 2000; received in revised form 28 February 2001; accepted 18 April 2001

Abstract

Cordierite ($Mg_2Al_4Si_5O_{18}$) ceramics are susceptible of mechanical failure due to their low fracture toughness, which may hinder their application. Dispersion of ZrO_2 in cordierite to improve the mechanical properties has been extensively studied. However, little is known about the effect of such additions on both the sinterability and the mechanical properties of cordierite bodies fabricated from talc, kaolin and alumina mixes with additions of monoclinic ZrO_2, as most studies are concerned with additions of tetragonal ZrO_2 to cordierite powders. The present paper describes the in situ fabrication, the thermal and mechanical properties of sintered cordierite-based ceramic matrix composites containing dispersed particles of ZrO_2 obtained by mixing clay–talc–alumina mixtures with additions of monoclinic ZrO_2 up to 40 wt.%. The results obtained clearly demonstrate that the thermal expansion coefficient (CTE), elastic moduli (E) and flexural strength (σ_r) were critically dependent on the mixing/milling conditions, the ZrO_2 content and the retained porosity.

Keywords: D. Cordierite; D. Zirconia; Ceramic matrix composites; Flexural strength; Thermal expansion coefficient

1. Introduction

Since its discovery by the French geologist Cordier in 1913, cordierite ($2MgO{\cdot}2Al_2O_3{\cdot}5SiO_2$) has been the subject of extensive research [1]. What makes cordierite most unique is its very low thermal expansion (as low as 7×10^{-7} K^{-1}, 25–1000 °C) which provides great resistance to thermal shock ($\Delta T > 350$ K).

Several cordierite-based ceramics and glass compositions have been developed and are being increasingly used in thermal–electrical applications where low thermal expansion and low dielectric permittivity ($\varepsilon_r \approx 4$ at 1 MHz) are critical [2], e.g. kiln furniture [1], electronic packaging [2] and substrates of catalysts for exhaust gas emissions control in automobiles [3].

Thermal shock resistance is one of the key requirements for ceramic honeycomb substrates coated with catalysts widely used for controlling automotive exhaust emissions. Cordierite combines relatively low thermal expansion (needed for thermal shock resistance) with relatively high refractoriness (needed for operating in severe exhaust environments at high temperatures). It is also inert to catalysts and the oxide coatings used as washcoats. Finally, it can be extruded into honeycomb substrates of suitable porosity and adequate mechanical strength. Nowadays, there are over 80 million substrates sold annually worldwide, making it one of the most significant ceramic products in the world [3].

Nowadays, it is well established that it is difficult to sinter pure cordierite bodies without any sintering aid. The use of sintering aids not only increases the thermal expansion coefficient but also deteriorates the dielectric characteristics of cordierite. Therefore, polycrystalline cordierite ceramics with high strength, high density and low thermal expansion coefficient (TEC) of stoichiometric composition, $2MgO{\cdot}2Al_2O_3{\cdot}5SiO_2$, are difficult to obtain because of the very narrow, impurity-sensitive firing range of this compound (within 25 °C of its incongruent melting point of 1455 °C) [4]. Commercial cordierite can be sintered to near full density at temperatures in excess of 1300 °C with the help of alkali oxides, typically K_2O, that promote liquid phase sintering. The resulting materials show low strength and low

* Corresponding author. Tel.: +351-217-164-211; fax: +351-217-166-568.

E-mail addresses: fernando.oliveira@imp.ineti.pt (F.A. Costa Oliveira), cruz.fernandes@ist.utl.pt (J. Cruz Fernandes).

0272-8842/02/$22.00
PII: S0272-8842(01)00061-X

fracture toughness, which limits their use in many potential structural applications. The strength–toughness relation is strongly dependent on the microstructure of the polycrystalline bodies.

It is widely accepted that the fabrication of composite materials is a rational strategy to design materials with properties that cannot be obtained for a monolithic material. Recently, several studies on the systems mullite–ZrO_2 [5] and cordierite–ZrO_2 [6–10] have shown that fine ZrO_2 dispersions in a ceramic matrix can affect the sinterability and considerably improve the mechanical properties of the composite. However, toughening of cordierite has been reported with ZrO_2 dispersion higher than 20 vol.% [6–10]. Such high ZrO_2 contents are likely to affect both the dielectric constant and the thermal expansion coefficient, which are the most advantageous properties of cordierite as electronic packaging substrate.

The goal of the present study was to examine the effect of additions of monoclinic zirconia (m-ZrO_2), up to 40 wt.%, on both the mechanical and thermal expansion properties of cordierite-based ceramics obtained by the conventional route (i.e. use of clay–talc–alumina mixtures), according to the methodology described elsewhere [11].

The thought that spawned the work described in this paper was that the addition of ZrO_2 to a cordierite composition developed in previous studies by the authors (composition *F* in Ref. [11]) would enhance densification and consequently improved mechanical properties could be attained as claimed by several authors [5–10].

In fact, it is widely accepted that transformation toughening usually involves stress-induced martensitic transformation of ZrO_2 particles from tetragonal (t-ZrO_2) to monoclinic (m-ZrO_2) symmetry in the stress field of a propagating crack; when such mechanism is operating both fracture strength and fracture toughness can be enhanced.

Upon heating, m-ZrO_2 undergoes a transformation into t-ZrO_2 at 1170 °C. Hence, the objective of adding m-ZrO_2 is to take advantage of this transformation to increase fracture toughness. Indeed, upon cooling from the sintering temperature, the t→m transformation is accompanied by a 3–5 vol.% expansion and thus residual stresses are created in the matrix by the presence of ZrO_2 particles. These stresses are known to affect the crack-tip stress field and thus influence the fracture toughness behaviour of the resulting bodies.

Dispersion toughening of oxide ceramics by t-ZrO_2 is a well-established process. Toughening mechanisms such as stress-induced transformation toughening, microcracking and crack deflection have been found to be responsible for improvement of the mechanical properties of such composites, as a result of the volume expansion associated with the t→m transformation. In some cases, however, the dispersed ZrO_2 particles were either very resistant to the transformation to the m-ZrO_2 or were unable to induce the stress-induced t→m transformation. For these reasons, dispersion of m-ZrO_2 rather than t-ZrO_2 additions was attempted. The only drawback of using m-ZrO_2 to improve toughness by the martensitic transformation mechanism is that ZrO_2 particles need to possess a critical size for retention of tetragonal phase to take place in the sintered bodies upon cooling. In addition, the amount of retained t-ZrO_2 is also dependent on the matrix constraint exerted on the zirconia particles. On the other hand, most of m-ZrO_2 can react with excess silica present in the mixes, at high temperatures (above 1280 °C), to form $ZrSiO_4$ [7]. However, even if the martensitic transformation toughening mechanism will not prevail, other toughening mechanisms like microcracking and crack deflection are expected to be active.

The results obtained in the present work are presented and discussed in terms of the relationship between the microstructure and the thermal–mechanical properties obtained.

2. Experimental procedure

The raw materials for all experiments were talc (Talco C74, Iberica de Talcos S.A., Leon, Spain, $d_{50} = 10$ μm), kaolin (Caulino MP, Cauliminas—Sociedade Mineira, S.A., Alcanede, Portugal, $d_{50} = 2.3$ μm), clay (Stoss-Ton No. 121, Theodor Stephan K.G., Haiger, Germany, $d_{50} = 2$ μm), feldspar (Dorkasil 70A, Gebroder Dorfner OHG, Hirschau, Germany, $d_{50} = 0.1$ μm), alumina (SC-B/01, Alumina Española S.A., Madrid, Spain, $d_{50} = 10$ μm) and silica (P6, Sibelco Portuguesa Lda., Rio Maior, Portugal, $d_{50} = 28$ μm). The samples were prepared in two stages. First, proportionate quantities of talc (30 wt.%), alumina (22 wt.%), clay (21 wt.%), kaolin (20 wt.%), feldspar (4 wt.%) and silica (3 wt.%) were wet mixed for 3 h. The slurry was dried at 120 °C for 24 h and sieved through a ASTM 125 μm mesh (the resulting mixture containing 52 wt.% SiO_2–35 wt.% Al_2O_3–10.5 wt.% MgO–1.5 wt% K_2O–0.5 wt.% Fe_2O_3– 0.5 wt.% TiO_2 is hereafter referred to as D). Then, additions of unstabilized ZrO_2 (monoclinic zirconia, Unitec Ceramics Ltd., Stafford, England, UK, $d_{50} = 0.58$ μm) in weight proportions of 10, 20, 30 and 40 wt% were made to the D mixture (hereafter these mixtures are denoted D10, D20, D30 and D40, respectively). Each lot was again wet mixed according to the procedure described above. After sieving, the resulting powders were uniaxially pressed at 50 MPa into 4.4×3.5×55 mm specimens for 4-point flexural strength measurements. Owing to the effect of particle size on densification of cordierite ceramics, all mixtures were also milled in an attrition mill for 1 h in distilled water at 4500 rpm using zirconia balls (hereafter these mixtures are referred to as DM,

D10M, D20M, D30M and D40M, respectively). In order to evaluate the effect of the milling time on the properties of the obtained cordierite, mixture D10 has been selected and milled for 5 h in the attrition mill under the same conditions as described above (hereafter this mixture is referred to as D10M 5h).

The compacts were sintered in air using a heating rate of 7 °C min^{-1}, soaked at 1250 °C for 1h and then cooled to room temperature at a rate of 2 °C min^{-1}. This heating schedule has been chosen to simulate sintering conditions normally found in industrial plants. Usually, cordierite–ZrO_2 composites are sintered at temperatures above 1300 °C (typically 1400 °C) [8,9]. Such higher firing temperatures allow denser materials to be obtained and consequently higher flexural strength and fracture toughness values than those reported in this paper.

Bulk density of the sintered samples was measured by the Archimedes method. For this purpose, the material was first made impermeable to the liquid (distilled water at room temperature) using a nitrate cellulose dope film of known density (1.3 g cm^{-3}).

True density measurements were carried out using a AccuPyc 1330 Helium pycnometer (Micromeritics Int. Corp., USA). Prior to the measurement, the as-sintered samples were ground in a WC mortar and dried at 150 °C under vacuum for 6 h.

Polished cross-section of samples with D and D10 compositions were observed on both a Philips XL30 FEG SEM and a Zeiss DSM 940 scanning electron microscope coupled with an energy dispersive X-ray (EDX—KEVEX Sigma) analyser for qualitative elemental analysis using both secondary electrons (SE) and back-scattered electrons (BSE) modes. Prior to examination, the samples were embedded in an epoxy resin and polished with a series of diamond pastes to 1 μm finish and then coated with a thin carbon layer to prevent surface charging during examination.

Phase identification and their relative intensities were ascertained by X-ray diffraction (XRD) using a Rigaku Geigerflex diffractometer (Rigaku Int. Corp., Japan) and CuK_α radiation. For this purpose, as-sintered samples were ground in an agate mortar and scanned over a range 2θ from 5 to 105°, at a scanning speed of 2° 2θ min^{-1}. Identification of the crystalline phases was carried out by comparison of the *d*-spacings and relative intensities obtained with those of reference material patterns compiled by the ICDD [12].

Flexural strength was determined using an Instron machine and a fully articulated jig with inner and outer spans of 20 and 40 mm, respectively, and a fixed crosshead speed of 0.5 mm min^{-1}. The flexural strength was calculated using the relationship:

$$\sigma_r = \frac{3F_r(S_1 - S_2)}{2bh^2} \quad (1)$$

where F_r is the maximum load recorded in the load vs. displacement graph; h is the specimen height (≈3 mm) accurately measured after each test; b is the specimen width (≈4 mm) accurately measured after each test; S_1 is the distance between external loading points (40 mm); S_2 is the distance between internal loading points (20 mm).

The different sets of data were treated using the two-parameter Weibull statistics. The general form of the Weibull cumulative distribution is given by

$$P = 1 - \exp\left[-\left(\frac{\sigma - \sigma_\mu}{\sigma_0}\right)^m\right] \quad (2)$$

where P is the fracture probability at stress σ, m is the shape parameter or Weibull modulus, σ_0 is the scale parameter or characteristic strength and σ_μ is the location parameter or threshold stress. When analysing fracture data of brittle materials with the Weibull distribution, σ_μ is usually set to zero and Eq. (2) can be simplified to give a two-parameter function that can be written as

$$y = \ln\ln\frac{1}{P_s} = m\ln\sigma_r - m\ln\sigma_0 \quad (3)$$

which represents a linear relationship between y and ln σ, with slope m. Hence, least squares' linear regression analysis can be performed on this equation.

The experimental definition of the survival probability (P_S) was done using the estimator [13]:

$$P_s = 1 - \frac{(i - 0.5)}{n} \quad (4)$$

where i is the rank of σ_r—value when all flexural strength results (of the same group of samples) are positioned in increasing order; n is the total number of results. This estimator has been shown to give the least biased estimation of m when $n > 20$ [13].

Prior to testing, the longitudinal edges of the samples (20 for each composition) were bevelled at ≈45°, using a diamond wheel, and very narrow chamfers were created.

Dynamic Young's modulus of sintered bodies was measured using an acoustic measuring device (Grindosonic MK5, J.W. Lemmens-Elektronika N.V., Leuven, Belgium) known as the impulse excitation technique, which gives the fundamental resonance frequency of flexural vibration of a sample after it has been excited by a light mechanical impulse (tap). The Young's modulus was calculated using the equation:

$$E = 0.9465\frac{\rho L^4 f^2 T}{t^2} \quad (5)$$

where L and ρ are the length and bulk density of the sample, f is the resonance frequency, T is a shape factor

(dependent on Poisson's ratio and the thickness, t, of the sample) [14,15]. The sample was supported at its nodes of resonance (0.224 L from each end) and tapped with samples of the material being tested as bead. A microphone located beneath the sample received the sound waves and passed the signal to an electronic box for Fourier analysis. Within a 3 s period, f was identified and then displayed in digital form. All calculations were done assuming a Poisson's ratio of 0.30.

The determination of the fracture toughness was made according to JIS R 1607 [16] from direct measurements of the crack traces on indented surfaces, using the indentation fracture theory for calculation purposes. In comparison with more conventional testing techniques, the indentation method offers a unique simplicity and economy in test procedure. The toughness was calculated using the equilibrium relation for K-field generated by the elastic-plastic contact of a Vickers' indentation on a brittle material for radial crack geometry, according to the following equation:

$$K_{\mathrm{Ic}} = 0.018\left(\frac{E}{H}\right)^{1/2}\left(\frac{P}{c^{3/2}}\right) \quad (6)$$

where E is the elastic modulus, H is the Vickers hardness, P is the indentation load and c is half of average of the crack length. This technique is suited to toughness evaluation on a comparative basis. However, it requires knowledge of the E/H ratio and the surface must be prepared to an optical finish, in order that crack sizes may be accurately measured. Precautions need to be taken in selecting an indentation load which satisfies the requirement that the pattern be well developed ($c \geqslant 2a$, with a being the dimension of the hardness impression) and that no chipping occurs.

Microhardness measurements were carried out according to ASTM E384 [17] using a Shimadzu HMV-2000 apparatus. The applied load was 1.96 N during 15 s, except in the case of mixture D10M 5 h where the load used was 2.94 N (due to difficulties in measuring the lengths of the crack traces). Polished cross-sections, ultimately with 1 μm diamond paste, were indented using a Vickers' diamond pyramid. Lengths of the crack traces of well-defined radial cracks and hardness diagonals from 10 indentations were measured using an optical microscope attached to the microhardness apparatus at a magnification of 2000×. Crack sizes were only measured for clearly defined radial traces and recorded within 60 s of indentation to avoid slow crack growth effects. Prior to the measurements, the test surfaces were coated with a thin layer of evaporated carbon in order to improve contrast and facilitate the crack length measurements.

The linear thermal expansion coefficients were measured in a dilatometer (Adamel-Lhomargy, model DM 15), according to the EN103 standard [18], with a heating rate of 5 °C min^{-1} from room temperature up to 600 °C, using sintered samples with a length of 65 mm.

3. Results and discussion

3.1. Apparent density and porosity of the sintered bodies

Table 1 shows the densities of the sintered cordierite obtained for the different mixtures prepared. The porosity is defined as $1-\rho_{\mathrm{bulk}}/\rho_{\mathrm{true}}$. Both the bulk and true densities of the composites increased with increasing ZrO_2 content (note that the theoretical density of cordierite is 2.51 g cm^{-3} whereas the density of m-ZrO_2 is 5.85 g cm^{-3} [5]). Also evident in Table 1 is that the porosity increased by a factor of ≈3 from 0 to 40 wt.% ZrO_2 content. Although it is apparent that the milling for 1 h resulted in a decrease of the apparent porosity of mixtures DM, D10 M and D20M in comparison with D, D10 and D20, the effect of milling on mixtures D30 and D40 is not seen. This suggests that the sintering temperature used for these compositions is far too low for obtaining dense cordierite bodies.

Fig. 1 shows the effect of the milling time on the specific surface area and the bulk density for mixture D10. For the D mixture, the mean specific surface area was 7.6 ± 0.1 m^2 g^{-1}, whereas as for DM a value of 8.8 ± 0.1 m^2 g^{-1} was obtained. Under the grinding conditions adopted in this study, both the average specific surface areas of the ground mixtures and the apparent densities increased with increasing grinding time. This result suggests that milling resulted in a finer mixture of the raw materials and hence specific surface area can be regarded as a critical parameter of the fabrication process. As the average particle size of the mixture becomes smaller than 0.19 μm (assuming that the particles are spherical) it can be concluded that it is possible to produce dense, pore-free cordierite ceramics from natural raw materials at temperatures as low as 1250 °C. For materials with

Table 1
Densities of sintered body compositions

Mixture	ρ_{bulk}[a] (g cm^{-3})	ρ_{true} (g cm^{-3})	Porosity (%)
D	2.49 (0.02)	2.70	7.8
D10	2.52 (0.03)	2.88	12.5
D20	2.54 (0.01)	3.16	19.6
D30	2.58 (0.02)	3.34	22.8
D40	2.65 (0.04)	3.65	27.4
DM	2.58 (0.02)	2.70	4.4
D10M	2.62 (0.03)	2.88	9.0
D20M	2.66 (0.01)	3.16	15.8
D30M	2.63 (0.02)	3.34	21.3
D40M	2.62 (0.03)	3.65	28.2
D10M 5h	2.80 (0.01)	2.88	2.8

[a] Standard deviations are shown in parentheses.

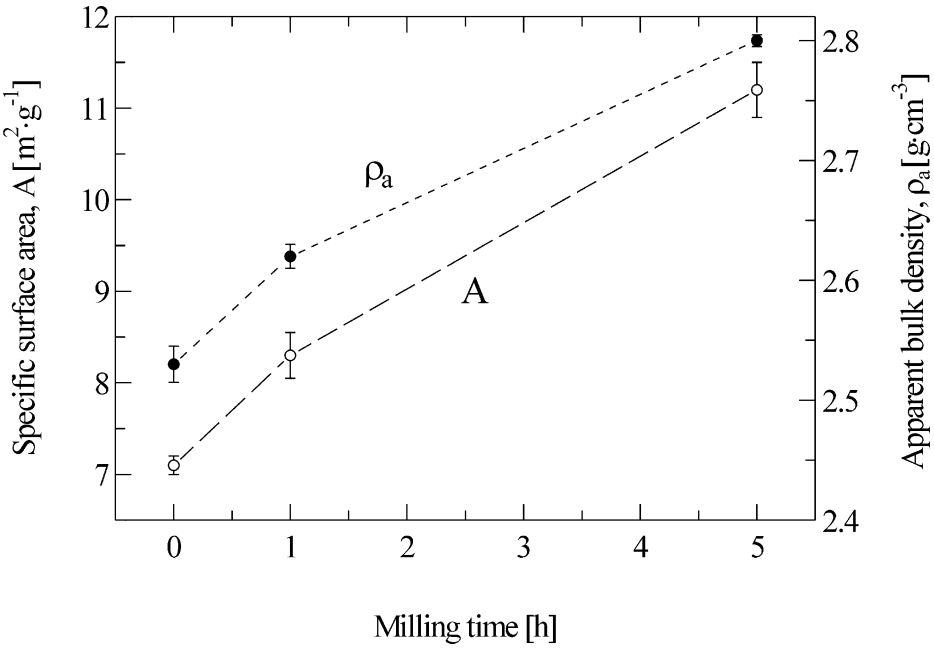

Fig. 1. Relationship between milling time and surface area of D10 mixtures and the resulting apparent bulk densities.

higher ZrO_2 contents, the firing temperature and the milling time need to be optimised in order to obtain denser materials. As illustrated in the present study, homogenous dispersion of ZrO_2 in cordierite is rather difficult to achieve, and hence alternative routes such as surface precipitation [9] should be envisaged.

The apparent porosity of the sintered bodies increased with increasing of the ZrO_2 content. In the case of mixtures which were not ground by attrition milling this can be attributed to a poor distribution of the ZrO_2 particles in the cordierite matrix (as illustrated in Fig. 4). This suggests that wet mixing for 3 h is not a suitable mixing step for obtaining high strength cordierite bodies, as it would be anticipated. However, it does provide a baseline for evaluating the effect of grinding on densification of cordierite ceramics. This study has also demonstrated that wet mixing should not be used to disperse ZrO_2 particles in kaolin, talc, alumina mixtures.

3.2. Microstructure of cordierite sintered bodies

In the sintered bodies obtained from mixtures containing ZrO_2 it was apparent that wet mixing did not result in homogenous powder mixtures, as large agglomerates of ZrO_2 particles were observed in the microstructure of these materials. The typical micrographs of as-polished surfaces can be seen in Figs. 2–4. The black areas correspond to pores in the microstructure. This seems to be a result of the insufficient mixing and grinding of raw materials.

Fig. 3 shows that the grain size of cordierite is not uniform and the morphology ranges from very small needle-like (less than 1 μm in diameter) to equiaxed

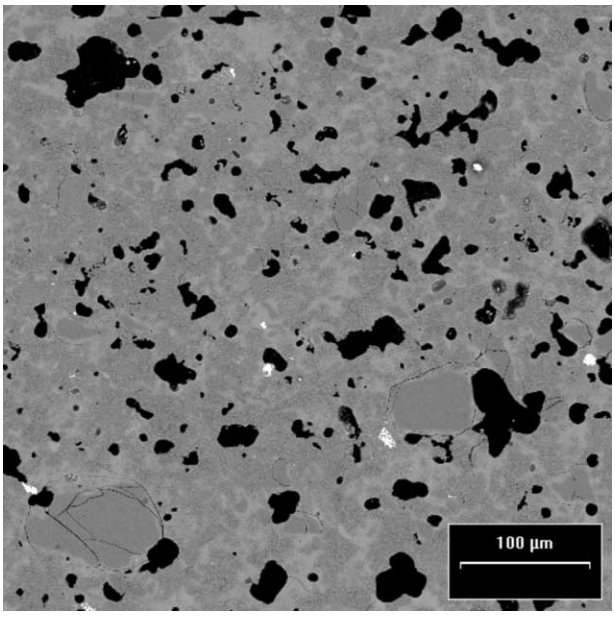

Fig. 2. Scanning electron micrograph of a polished cross-section of composition D.

grains. It is likely that most α-cordierite grains were nucleated from a liquid phase formed by melting of talc particles. EDX analyses revealed that the matrix consists of two main phases: the lighter areas (possibly a glassy phase) consisting of Si, O and traces of Al, K, Ca and Mg (impurity present in the raw materials); the darker areas were found to contain Si, Mg, Al and O (possibly the cordierite phase). At higher magnifications, EDX analysis performed on crystals of the needle-like type showed them to consist of Al, Si, Mg and

O (indicating that they are most likely α-cordierite). Evidence of Al_2O_3 crystals was also depicted by EDX analysis. The white areas in Fig. 4 were found by EDX to consist of agglomerates of ZrO_2 particles and hence ZrO_2 is not homogeneously distributed within the matrix (cordierite mean grain size less than 2 μm). It can therefore be concluded that the mixing of the raw materials is a critical step to produce a dense, high-strength cordierite body. Finally, large particles (about 50 μm on average) found by EDX to be SiO_2, were observed (dark grey areas usually cracked, since quartz particles contract more than the matrix). These observations are in good agreement with evidence gathered by XRD analysis (see below).

Figs. 5 and 6 show that attrition milling has resulted in a denser and finer microstructure (compared to that seen in Fig. 4) and a more homogenous distribution of Zr within the matrix (Zr-rich particles correspond to the white areas shown in Figs. 5 and 6). Most of the pores observed in Fig. 6(a) are smaller than 2 μm and spherical in shape. These SEM micrographs indicate that there is good agreement between these observations and the experimental data for apparent porosity shown in Table 1. It can also be seen in Fig. 5(b) that the grain size of the α-cordierite crystals is not uniform and is below 2 μm. These crystals seem to have nucleate from a glassy phase. Some of them might have grown in the liquid phase formed by melting of the talc particles, which facilitated liquid phase sintering. Also seen in Fig. 5 is that some Zr-rich particles are actually particle clusters indicating some agglomeration has still occurred but at considerable less extent than that observed in Fig. 4.

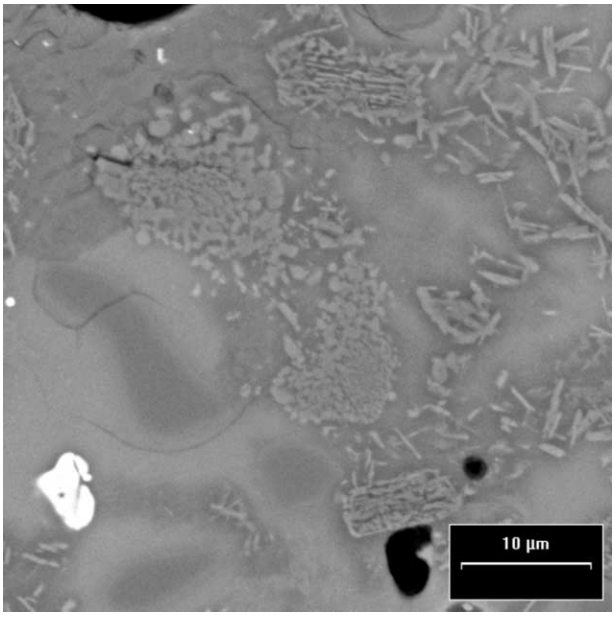

Fig. 3. Scanning electron micrograph of a polished cross-section of composition D at a higher magnification.

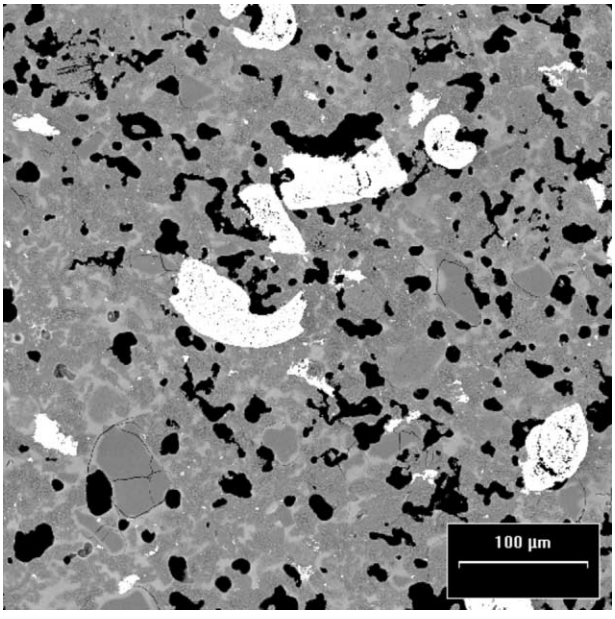

Fig. 4. Scanning electron micrograph of a polished cross-section of composition D10.

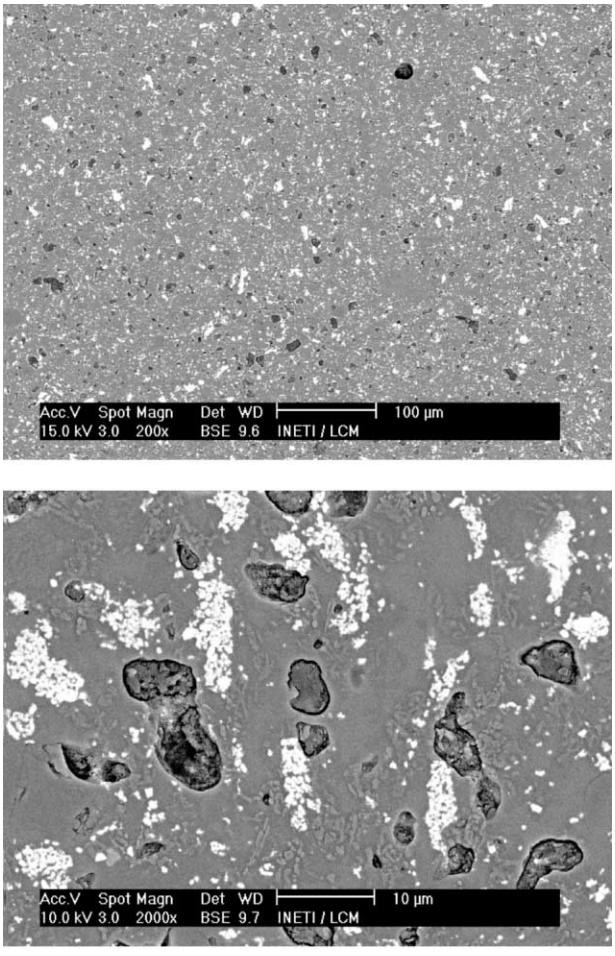

Fig. 5. Scanning electron micrographs of polished cross-sections of sintered bodies of D10M (above) BSE image showing main microstructural features and (below) BSE image at a higher magnification.

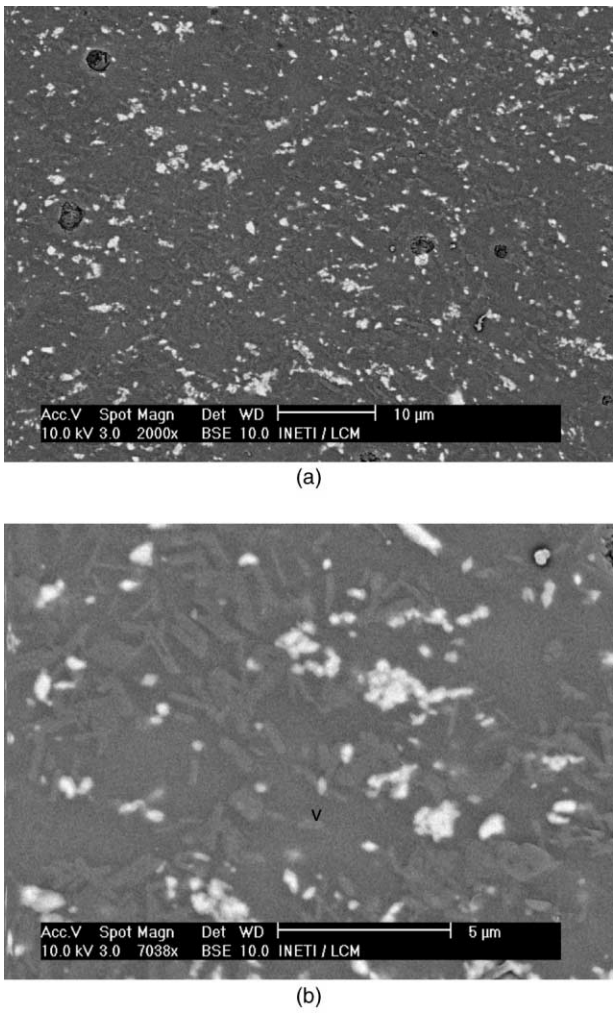

Fig. 6. Scanning electron micrographs of polished cross-sections of sintered bodies of D10M 5h (a) SE image and (b) BSE image at a higher magnification.

3.3. X-ray diffraction analysis of sintered bodies

XRD analysis of the as-sintered composites revealed that the addition of ZrO_2 has resulted in the formation of zircon ($ZrSiO_4$, tetragonal, ICDD card No. 06-0266) in a indialite (synthetic cordierite, α-$Mg_2Al_4Si_5O_{18}$, hexagonal, ICDD card No. 13-0293) matrix. In addition, traces of sapphirine ($Mg_4Al_8Si_4O_{20}$, monoclinic, ICDD card No. 19-0750), corundum (α-Al_2O_3, rhombohedral, JCPDS card No. 10-0173), quartz (α-SiO_2, hexagonal, ICDD card No. 46-1045), spinel ($MgAl_2O_4$, cubic, ICDD card No. 21-1045), and baddeleyite (ZrO_2, monoclinic, ICDD card No. 37-1484) were also depicted (as shown in Figs. 7–9). Both Figs. 7 and 8 show an increase in cordierite content as a result of attrition milling (higher relative intensities were recorded for compositions DM and D10M). Also seen in these figures is that the content of α-SiO_2 and α-Al_2O_3 decreased in the case of DM and D10M and the zircon content increased in the case of D10M.

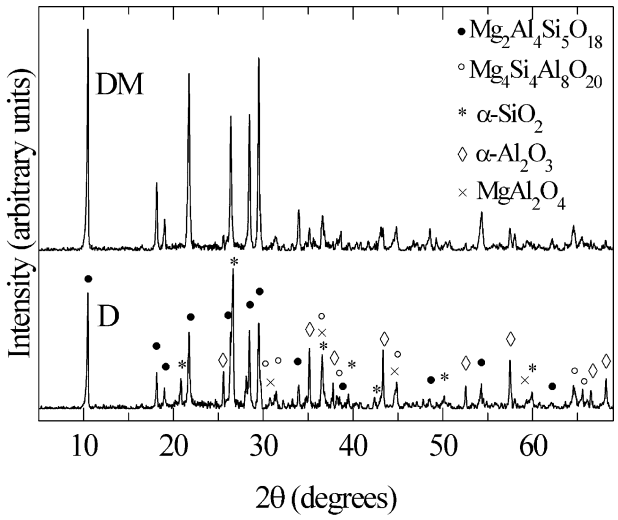

Fig. 7. X-ray diffraction patterns of the samples D and DM.

Therefore, attrition milling has resulted in an improvement of the sinterability of these compositions (as also indicated by the decrease in porosity shown in Table 1). As the particle size of the ground mixtures becomes smaller with increasing of the milling time, the formation of α-cordierite takes place at lower temperatures and at a greater extent. Nakahara et al. [19] reported that dense sintered bodies were obtained by firing ground mixtures of calcined kaolin, calcined talc and alumina with particle size of 0.39 μm (corresponding to a grinding time of 120 h) or smaller at temperatures as low as 1200 °C.

The peak intensity of cordierite (maximum intensity peak (110) corresponds to $2\theta = 10.46°$) increases with increasing of the milling time (Fig. 8). The increase of reactivity observed for mixtures prepared by attrition milling can also be related to a more homogenous mixing of the raw materials. While α-cordierite content increases, the amounts of sapphirine, alumina, quartz and spinel decrease. The small amount of sapphirine might have resulted from an alumina-rich composition in comparison with the theoretical cordierite composition.

Fig. 9 shows a continuous decrease in cordierite content and increase in zircon content with increasing ZrO_2 addition. This is in good agreement with experimental evidence gathered elsewhere [7,20] showing that ZrO_2 reacts with cordierite to form zircon ($ZrSiO_4$) and spinel ($2MgAl_2O_4$). This chemical reaction was found to occur preferably at temperatures above 1280 °C [6], with the amount of these phases increasing with increasing of the sintering temperature and prolonged holding times.

The presence of tetragonal ZrO_2 was not detected in the XRD patterns in Figs. 8 and 9. Upon heating m-ZrO_2 is expected to transform into tetragonal ZrO_2 (t-ZrO_2) at 1170 °C [21]. On cooling, the reverse t→m transformation is expected to occur, although it could

be argued that tetragonal zirconia phase would be thermodynamically stable unless its size is higher than a critical value [8]. It could also happen that the amount of retained t-ZrO_2 is smaller than the detection limit of the XRD equipment. TEM investigations by means of electron diffraction analysis are required to elucidate on this matter.

Finally, as illustrated in Fig. 4, the distribution of ZrO_2 particles within the matrix was not homogenous, i.e. large agglomerates were observed. Due to the t→m transformation of the ZrO_2 agglomerates on cooling "macro" cracks have resulted. Hence, a more effective mixing method, either ball milling or attrition milling, should be used if dense and pore-free sintered bodies are to be obtained.

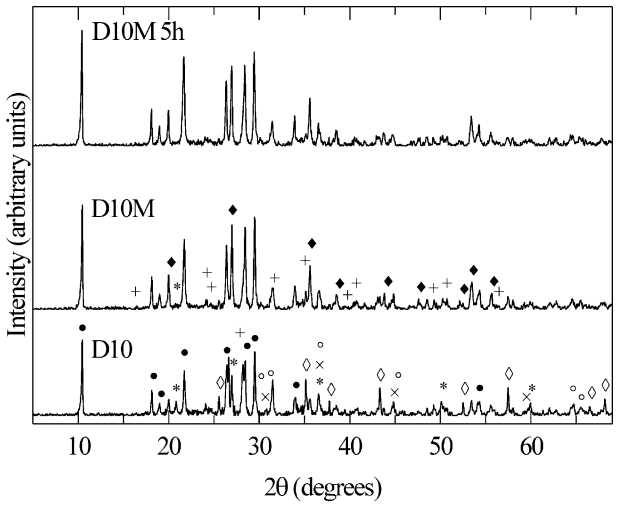

Fig. 8. X-ray diffraction patterns of samples, D10, D10M and D10M 5 h. (●, $Mg_2Al_4Si_5O_{18}$; ○, $Mg_4Al_8Si_4O_{20}$; ◆, $ZrSiO_4$, + ZrO_2; ∗, α-SiO_2; ◇, α-Al_2O_3; ×, $MgAl_2O_4$).

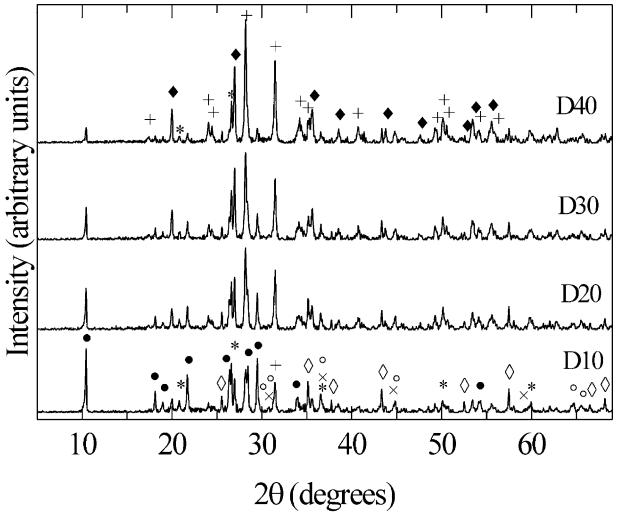

Fig. 9. X-ray diffraction patterns of the samples D10, D20, D30 and D40 (●, $Mg_2Al_4Si_5O_{18}$; ◆, $ZrSiO_4$, + ZrO_2; ○, $Mg_4Al_8Si_4O_{20}$; ∗, α-SiO_2; ◇, α-Al_2O_3; ×, $MgAl_2O_4$).

3.4. Bending strength and elastic moduli of the sintered bodies

The mechanical properties of the cordierite and ZrO_2-containing composites sintered at 1250 °C are shown in Figs. 10 and 11. Fig. 10 shows that the 4-point bending strength, σ_r, and the elastic modulus, E, decrease with increasing ZrO_2 content. This behaviour is closely related to the microstructure obtained, as strength decreases with increasing porosity (see Table 1). The presence of some "macro" cracks resulting from phase transformation of the both ZrO_2 agglomerates and large quartz particles present in the composites is also expected to contribute for the degradation of the mechanical strength of the sintered bodies obtained.

Fig. 11 shows the effect of the zirconia content on both σ_r and E of sintered bodies obtained from mixtures that were prepared by attrition milling for 1 h. It can

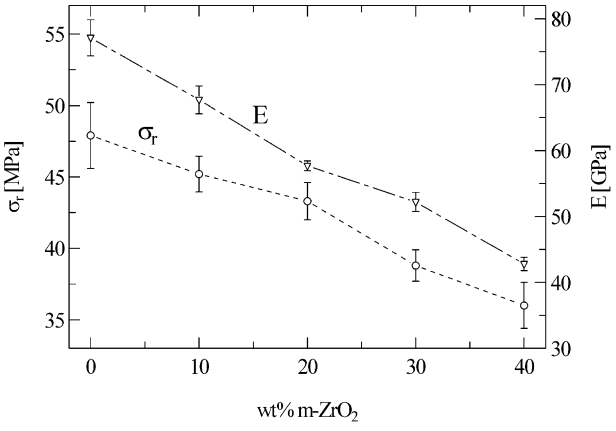

Fig. 10. Effect of zirconia content on mechanical strength of cordierite bodies obtained from wet mixed mixtures.

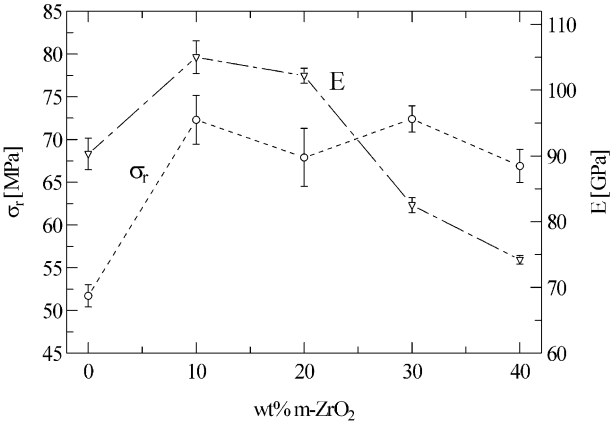

Fig. 11. Effect of zirconia content on σ_r and E of cordierite bodies obtained from ground mixtures for 1 h milling time.

clearly be seen that the addition of ZrO_2 results in a significant increase of σ_r (about 40%). It is also noted that additions of ZrO_2 higher than 10 wt.% resulted in a small effect on σ_r, despite the fact that the porosity content increased with increasing ZrO_2 content (see Table 1). This suggests that attrition milling has not changed the pores content considerably (except for mixture D10M 5 h), but has altered the morphology of the pores, as they become smaller and spherical in shape and there are less agglomerates and smaller quartz particles (see Figs. 5 and 6). In Fig. 11, it is also seen that E increased from 90.3 ± 4.8 to $105. \pm 5.0$ GPa with increasing ZrO_2 content from 0 to 10 wt% (as expected from the rule of mixtures, assuming that the elastic modulus of ZrO_2 is around 200 GPa) and then decreased with increasing porosity, particularly for the higher ZrO_2 contents, as it would be expected. Table 2 summarises the main properties of the sintered bodies obtained in this study.

Fig. 12 shows the effect of milling time on σ_r and E of sintered bodies obtained from mixture D10. A significant increase in strength was observed for composition D10M 5 h as compared to D10 (factor of 2), as a result of attrition milling. This indicates that the mechanical properties of these composites are closely related to the particle size of the raw materials ground by attrition milling.

Fig. 13 shows a Weibull plot illustrating this finding. The larger scatter in data obtained for mixture D10M 5h (and consequently the lower value of m recorded) is attributed to difficulties in die-pressing resulting from a decrease of the particle size. It was necessary to increase the filling height (by a factor of about 2) to ensure samples' height in accordance to the standard ≈3 mm. This resulted in some bending of the green bars, which was not possible to correct during sintering. Therefore, a binder should have been used to facilitate die-pressing avoiding this problem to occur. For comparison purposes, it was decided not to add a binder to the system. In practice this problem can be minimised by granulating the ground powder prior to pressing.

Flexural strength seems therefore to be closely related to the microstructure of the composites. The key parameters that determine the fracture strength of brittle materials are the fracture energy, the Young's modulus and the critical defect size. Hence, a homogenous distribution of the ZrO_2 particles in the cordierite matrix is expected to influence the fracture strength. On the other hand, strength is also dependent on the size and distribution of the critical defects (e.g. pores and cracks).

Based on density data (Table 1), the decrease in apparent porosity of mixture D10M in comparison with D10 (≈28% does not justify alone this improvement in strength. The explanation for this finding must be related to: (i) the formation of a stronger $ZrSiO_4$ phase [22]; (ii) the effect of ZrO_2 on the fracture toughness of the composite, i.e. milling has resulted in a finer distribution

Table 2
Properties of the sintered compositions

Mixture	CTE[a] ($K^{-1} \times 10^{-6}$)	σ_r[b] (MPa)	E[b] (GPa)	m[c]
D	5.7	47.9 (4.6)	77.1 (5.5)	11.2
D10	4.7	45.2 (2.5)	67.7 (4.2)	21.6
D20	4.9	43.3 (2.6)	57.7 (1.5)	19.9
D30	5.2	38.2 (2.2)	52.2 (2.9)	21.1
D40	5.5	36.0 (3.2)	42.8 (2.0)	13.2
DM	4.4[d]	51.6 (2.6)	90.3 (4.8)	24.2
D10M	4.2	72.3 (5.7)	105.0 (5.0)	15.1
D20M	–	67.9 (6.8)	102.2 (2.3)	11.9
D30M	–	72.4 (3.1)	82.5 (2.3)	27.7
D40M	–	66.9 (3.9)	74.2 (1.3)	20.5
D10M5h	–	92.5(14.5)	119.2 (1.0)	6.4

[a] Mean coefficient of thermal expansion between 298 and 873 K.
[b] Standard deviations, σ_{n-1} are indicated in parentheses.
[c] $n = 20$ in all cases.
[d] Coefficient of thermal expansion in the range of 473 to 873 K.

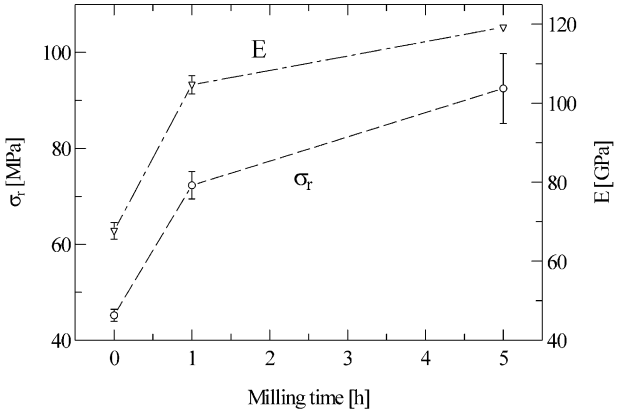

Fig. 12. Effect of milling time on the flexural strength and the elastic modulus of mixture D10.

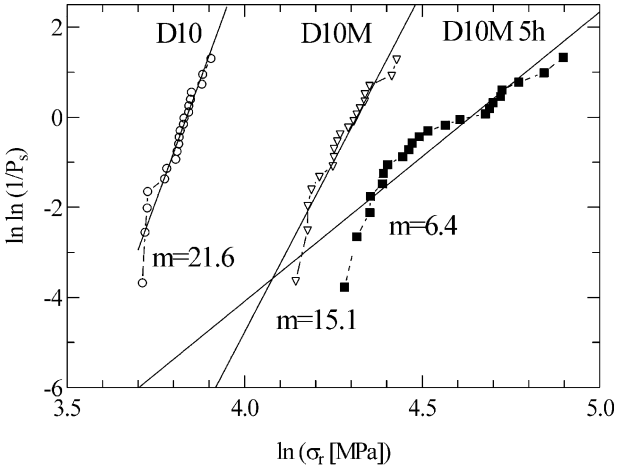

Fig. 13. Weibull graph showing the results for samples D10 and D10M.

of the ZrO_2 particles in the matrix; and (iii) the size reduction of the quartz particles.

The high Weibull moduli recorded (see Table 2), suggests that the distribution of critical defects of the tested materials is very narrow.

To achieve maximum strength, it is essential to assure a homogeneous distribution of the fine (≈1 μm) ZrO_2 particles within the matrix and to minimise the porosity. This can be done by optimising both the mixing and the sintering cycle steps, respectively. During sintering, two temperature dependent processes occur which influence the porosity: the viscosity of the transient glassy phase formed on heating and the crystallisation kinetics. The heating cycle must be controlled in such a way that the samples are sintered to a high density prior to crystallisation takes place. Otherwise, the viscosity rapidly increases and, consequently, the sintering mechanism changes from viscous to diffusive, which requires a much higher fabricating temperature. Further work needs to be carried out in order to gain a better understanding of the sintering mechanisms involved in the densification of the cordierite–ZrO_2 composites obtained by the proposed in situ fabrication route—which was not in the scope of the present work. The use of the rate-controlled sintering method instead of the conventional temperature sintering should be envisaged and optimisation of the sintering cycle should be sought by evaluating the densification kinetic data and the observed microstructures [23].

3.5. Thermal expansion coefficient of cordierite bodies

Ceramics based on cordierite usually possess relatively low polycrystalline linear thermal expansion, ranging from 1×10^{-6} to 4×10^{-6} K^{-1}, owing to the fact that the lattice thermal expansion coefficient in the *c*-direction of thehexagonal α-cordierite (known as indialite) is negative [27]. Alkali substitution will affect lattice parameters thereby influencing the thermal expansion [26]. The differences in the expansions of single crystals and the polycrystalline materials suggest that unrecognised constraints of physical origin affect the expansion of polycrystalline materials. Since each particle of the polycrystalline material contains many crystallites, the average crystallite expansions are likely affected by such constraints. Hence, the thermal expansion behaviour is very sensitive to the chemistry and the atomic packing arrangement being dependent on both the fabrication conditions and composition changes. On the other hand, particles of larger thermal expansion coefficient (TEC), e.g. α-Al_2O_3, cristobalite and $ZrSiO_4$, in a matrix of lower TEC cause thermal strain (tension) resulting in the genesis of microcracks in the matrix around the particles during heating and cooling cycles. When this happens, hysteresis of the thermal expansion curves is observed as microcracks generation during cooling results in a decrease of thermal expansion.

The thermal expansion coefficients for the sintered cordierite bodies obtained are shown in Table 2, which were measured for the temperature range of 20 to 600 °C. It should be noted that the standard deviation of the CTE data reported in this table is $\pm0.1\times10^{-6}$ K^{-1}, based on five measurements made using a Al_2O_3 reference material. In the case of DM, the thermal expansion curves were not linear upon heating. A change in slope was observed at around 200 °C. The reason for this change of slope is due to the presence of cristobalite possibly formed by the crystallisation of amorphous silica decomposed from kaolin and talc. As illustrated by Fig. 14, when cristobalite is present, a change in slope may be attributed to an expansion of cristobalite at temperatures close to 200 °C.

The thermal expansion behaviour was also influenced by the ZrO_2 addition, with the coefficient of linear thermal expansion increasing with increase in ZrO_2 addition (Table 2 and Fig. 15). This is explained by the presence of phases with higher expansion coefficients (zircon, ZrO_2, sapphirine, alumina, spinel) than cordierite. For instance, the average thermal expansion coefficient of sapphirine is $\approx8.9\times10^{-6}$ K^{-1} in the 20–800 °C temperature range [25], significantly higher than that of cordierite ($1–2\times10^{-6}$ K^{-1} between room temperature and 1000 °C) [26].

Cordierite has the lowest thermal expansion coefficient of all the crystalline phases in the three-oxide system $MgO–Al_2O_3–SiO_2$ [2]. To minimise thermal expansion and thus maximise thermal shock resistance, compositions as close as possible to that of cordierite are required. Our results clearly demonstrate that an increase of the level of reactivity, e.g. achievable through the use of attrition milling, results in more cordierite being formed and, consequently, in a lower CTE (see Table 2). The reason why the CTE of D is higher than all the others can be explained by comparing the relative intensities of the main diffraction peaks obtained under the same scanning conditions. In fact, XRD data suggests that the composition D contains

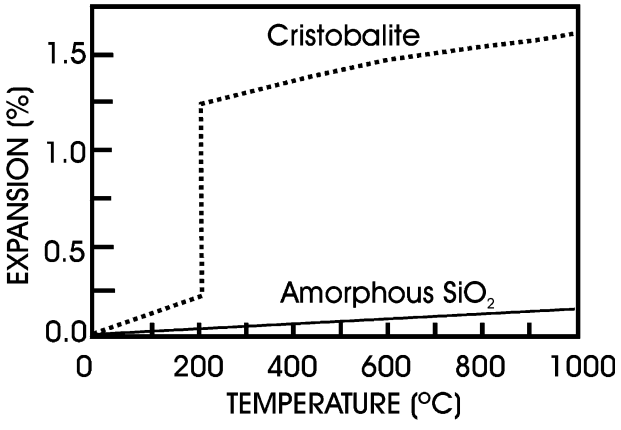

Fig. 14. Thermal expansion of silica versus temperature [24].

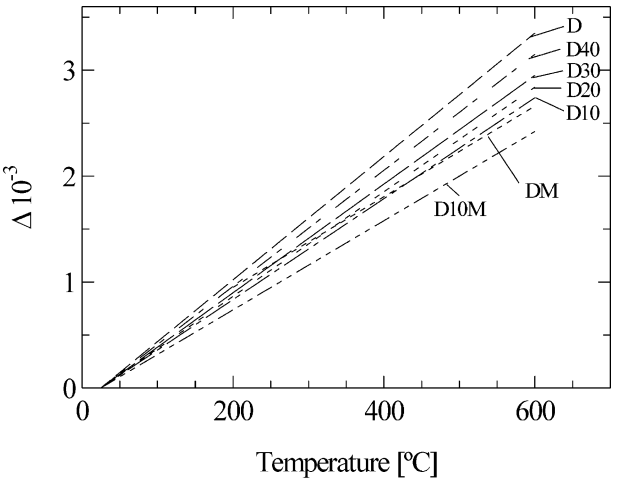

Fig. 15. Thermal expansion (Δ) as a function of temperature.

slightly higher contents of α-SiO_2 (CTE of 11.2×10^{-6} K^{-1} in the 20 to 200 °C temperature range [2]) and α-Al_2O_3 (CTE of 6.5×10^{-6} K^{-1} in the 20 to 200 °C temperature range [2]) than composition D10, as shown in Figs. 3 and 4, respectively. The presence of these phases can thus contribute to a larger CTE being recorded. On the other hand, for the composite materials, the reaction between SiO_2 and ZrO_2 to form $ZrSiO_4$ leads to a decrease of the free SiO_2.

Thermal expansion also depends on the glass composition, and expansion is increased mostly by alkali oxides ($9.0–9.6\times10^{-6}$ K^{-1}) [5]. Additions of such oxides must be therefore kept to a minimum. The impurities in the starting materials can also enter the cordierite lattice as dopants and influence the thermal properties. Hence, the alkali content of the raw materials should be controlled: low alkali content is important for low expansion. Calcium oxide, a common impurity in talc, also affects thermal expansion [27]: the expansion coefficient increases with calcium oxide content. On the other hand, firing rate can also affect the thermal expansion coefficient as it may influence the degree of cordierite formed.

Since the measurement of the CTE was made on sintered polycrystalline samples, the anisotropy in thermal expansion as reported by other authors [28–30] is not seen. In fact, the small thermal expansion coefficient of α-cordierite is partly related to its thermal expansion anisotropy. On heating, cordierite shows a small thermal expansion in the direction of the *a*-axis and a small contraction in the direction of the *c*-axis. Hence, thermal expansion may be affected by the porosity content, as it is believed that such expansion and contraction of the cordierite crystal can easily occur in sintered bodies of higher porosity. This could explain why the thermal expansion coefficients of denser cordierite bodies are slightly higher than those with higher residual porosity.

In order to minimise the CTEs, the reaction of ZrO_2 with cordierite to form zircon (note that CTE of $ZrSiO_4$ is 4.1×10^{-6} K^{-1} [31]) and spinel needs to be limited. This can be achieved by adding ZrO_2 doped with yttria (e.g. 3 mol% Y_2O_3–PSZ) instead of unstabilised m-ZrO_2 [7,10].

3.6. Fracture toughness of sintered bodies

In general, cordierite materials show low fracture toughness (1.5 to 2.3 MPa $m^{\frac{1}{2}}$) and the highly flaw-sensitive strength of these materials at room temperature limits their use in many structural applications. Owing to the thermal expansion anisotropy effects of cordierite discussed above, it is likely that expansion and contraction of the cordierite crystallites will result in constraints which may lead to residual stresses and ultimately microcracks. These, in turn, will affect the fracture behaviour of the polycrystalline materials. In the present work we aimed at increasing the room temperature fracture toughness of cordierite-based ceramics by using toughening mechanisms such as stress-induced transformation toughening, microcracking and crack deflection through the addition of a zirconia second phase. This approach has been successfully employed to improve the mechanical properties of alumina, mullite and spinel taking advantage of the thermal-expansion-mismatch stresses between the matrix and the second phase. The in situ toughening route offers the possibility of fabricating complex shapes and large size components and high reinforcement-phase volume fraction. These advantages can contribute to considerable saving in the cost of a component making this approach an attractive one for producing tougher cordierite bodies.

Table 3 summarises the fracture toughness results obtained for materials fabricated under different conditions.

The mean values of Vickers' hardness obtained between 7.3 and 8.2 GPa are similar to those found in the literature for cordierite ceramics (8.2 GPa) [32]. The larger scatter in the data was recorded for the materials yielding higher porosity contents.

The lower values of K_{Ic} determined on the sintered bodies compared with data reported in the literature (1.65–2.9 MPa $m^{\frac{1}{2}}$ for pure cordierite) [32,33] suggests that the addition of ZrO_2 had little effect on the fracture toughness. However, it is noted that the fracture toughness increases slightly with increasing milling time. This is probably related to the effect of milling on the microstructures obtained.

Several toughening mechanisms may occur simultaneously in ZrO_2-toughened cordierite composites. A crack bowing and/or a crack deflection mechanisms can contribute somewhat to the relative increase of K_{Ic} (see Table 3). Another mechanism that can also be important in toughening of cordierite–zirconia composites is

Table 3
Fracture toughness and hardness (1.96 N) of sintered bodies

Mixture	H_V[a] (GPa)	K_{Ic}[a] (MPa $m^{1/2}$)
D	7.34 (1.25)	0.9 (0.1)
DM	8.16 (0.60)	1.4 (0.2)
D10	7.28 (1.94)	0.9 (0.1)
D10M	7.99 (0.74)	1.5 (0.1)
D10M 5h[b]	8.08 (0.28)	1.9 (0.1)

[a] Mean and standard deviation (in parentheses) of 10 measurements.
[b] Applied load 2.94 N.

microcracking due to the presence of residual stresses. The lower thermal expansion of cordierite compared with that of zirconia leads to tensile stresses being imposed on zirconia particles during cooling. These stresses may lead to microcracking around the transformed m-ZrO_2 inclusions. Although in some cases ZrO_2 phase was found to remain tetragonal on cooling as in Ref. [20], even though the starting ZrO_2 powder had only monoclinic phase, this has not been the case in the present study. Hence, it is believed that stress-induced transformation toughening is not an important mechanism in these particular composites. Unfortunately, the microstructure of the sintered materials was not very homogeneous making it difficult to determine the fracture toughness by the indentation method and to observe some microcracks by SEM at high magnifications. A more detailed discussion would require TEM observations in order to investigate whether microcracking around the transformed monoclinic zirconia particles has occurred or not. In any case, it is expected that transformation-induced microcracking toughening is the most likely active mechanism responsible for some of the observed increase in toughness of these zirconia-toughened cordierite composites.

4. Conclusions

Composites in the system cordierite–ZrO_2, prepared by mixing talc–clay–alumina mixtures with unstabilised ZrO_2, offer promising properties in both enhancing the sinterability of cordierite and improving mechanical properties of cordierite.

The densities of the composites are affected by the milling times and increasing of ZrO_2 content has resulted in higher porosity contents. For some compositions (e.g. D and D10), attrition milling of the raw materials has resulted in an increase in cordierite content and a decrease in porosity leading to lower CTE values as well as in a more homogenous distribution of the ZrO_2 particles in the matrix. When attrition milling was not used, elastic modulus and flexural strength of the composites were degraded by increasing the ZrO_2 content. This is related to an increase in the residual porosity and "macro" crack enhancing. The thermal expansion behaviour was also influenced by the ZrO_2 addition, with the mean coefficient of thermal expansion increasing with increase in ZrO_2 addition, owing to the appearance of phases with higher expansion coefficients than cordierite and the decreasing of the volume fraction of cordierite formed.

The addition of ZrO_2 induced the formation of $ZrSiO_4$ thus affecting densification, which resulted in substantial improvement in strength in the case of D10M composition as compared to DM. This suggests that additions of ZrO_2 play an important role in improving the mechanical properties of cordierite–ZrO_2 composites, providing that optimum milling conditions of the raw materials are used.

The thermal expansion coefficient of the composites is mainly determined by the volume fraction of the cordierite formed. Attrition milling has resulted in higher cordierite contents and consequently lower CTE values.

Additions of ZrO_2 resulted in improvements of strength and elastic moduli for the composites prepared by attrition milling. Such improvements were to be expected as the ZrO_2 has a higher strength and rigidity than cordierite. Improvements were also observed with increasing milling times, as a result of a reduction of particle size and a more homogenous distribution of the ZrO_2 particles. Dense cordierite bodies were obtained at temperatures as low as 1250 °C. Finally, fracture toughness was also affected by milling time, increasing with increase of milling time, as a result of a better distribution of the ZrO_2 particles and particle size reduction. Transformation-induced microcracking toughening is most likely the mechanism responsible for some of the increase in toughness observed.

Acknowledgements

The authors thank the valuable technical assistance given by A. Cardoso (density measurements, die-pressing and cold isostatic pressing) and T. Magalhães (XRD), L. Soares (ceramography), P. Coelho (microhardness), M.J. Matos (SEM) at INETI and P. Amaral (4-point bending tests) at IST. The technical support of K. Schuster (SEM) and P. Frampton (ceramography) from the Joint Research Centre of the European Commission in Petten, The Netherlands, is also acknowledged. We also thank D. Dias of Rauschert Portuguesa, Lda. for supplying most of the raw materials used in this work.

References

[1] P. Grosjean, Chlorite and chlorite-rich talcs in cordierite, Interceram. 44 (6) (1995) 411–414.

[2] R.R. Tummala, Ceramic and glass-ceramic packaging in the 1990s, J. Am. Ceram. Soc. 74 (5) (1991) 895–908.
[3] P.M. Then, P. Day, The catalytic converter ceramic substrate—an astonishing and enduring invention, Interceram. 49 (1) (2000) 20–23.
[4] R. Morrell, The mineralogy and properties of sintered cordierite glass-ceramics, Proc. Br. Ceram. Soc. 28 (1979) 53–71.
[5] K. Das, S.K. Das, B. Mukherjee, G. Banerjee, Microstructural and mechanical properties of reaction-sintered mullite–zirconia composites with magnesia as additive, Interceram. 47 (5) (1998) 304–312.
[6] K. Nieszery, K.L. Weisskopf, G. Petzow, W. Pannhorst, Sintering and strengthening of cordierite with different amounts of zirconia, in: P. Vincenzi (Ed.), High Tech Ceramics, Materials Science Monographs, vol. 38A, Elsevier Science Publishers B.V., Amsterdam, The Netherlands, 1987, pp. 841–849
[7] N.A. Travitzky, N. Claussen, Chemical stability of cordierite-ZrO_2 composites, J. Eur. Ceram. Soc. 5 (1989) 327–331.
[8] I. Wadsworth, J. Wang, R. Stevens, Zirconia toughened cordierite, J. Mater. Sci. 25 (1990) 3982–3989.
[9] H.M. Jang, Surface precipitation route for the development of cordierite–zirconia composites, J. Am. Ceram. Soc. 78 (3) (1995) 723–727.
[10] A. Das Gupta, P.S. Sen, M.K. Sinha, M.K. Basu, Effect of ZrO_2 addition on strength and dilatation behaviour of cordierite ceramics, J. Mater. Sci. Lett. 13 (1994) 332–334.
[11] F. Oliveira, J.J. Fernandes, L.G. Rosa, Obtenção e caracterizaçamicos à base de cordierite, in: A.M. Segadães (Ed.), Interactions in Materials, Proceedings of the 7th National Meeting of the Portuguese Materials Society, vol. 1, 1995, pp. 375–382.
[12] Powder Diffraction File: PDF-2, Database sets 1-47, International Centre for Diffraction Data (ICDD), Pennsylvania, USA, 1997.
[13] A.D. Papargyris, Estimator type and population size for estimating the Weibull modulus in ceramics, J. Eur. Ceram. Soc. 18 (1998) 451–455.
[14] S. Spinner, W.E. Tefft, A method for determining mechanical resonance frequencies and for calculating elastic moduli from these frequencies, Proc. ASTM 61 (1961) 1221–1238.
[15] ASTM C1259-96, Standard Test Method for Dynamic Young's Modulus, Shear Modulus, and Poisson's Ratio for Advanced Ceramics by Impulse Excitation of Vibration, 1996, pp. 374–382.
[16] JIS R 1607, Japanese Industrial Standard, Testing Methods for Fracture Toughness of High Performance Ceramics, 1990.
[17] ASTM E384, Standard Test Method for Microhardness of Materials, 1990, pp. 385–402.
[18] EN 103, Determinazione della dilatazione termica lineare di piastrelle di ceramica, 1991.
[19] M. Nakahara, Y. Kondo, K. Hamano, Effect of particle size of powders ground by ball milling on densification of cordierite ceramics, J. Ceram. Soc. Japan 107 (4) (1999) 308–312.
[20] B. Lim, H.M. Jang, Homogeneous fabrication and densification of cordierite–zirconia composites by a mixed colloidal processing route, J. Am. Ceram. Soc. 76 (6) (1993) 1482–1490.
[21] K.K. Srivastava, R.N. Patil, C.B. Choudhary, K.V.G.K. Gokhale, E.C. Subbarao, Revised phase diagram of the system ZrO_2–$YO_{1.5}$, Trans. J. Br. Ceram. Soc. 73 (3) (1974) 85–91.
[22] R. Morrell, Handbook of Properties of Technical and Engineering Ceramics, Part 1 An Introduction for the Engineer and Designer, Her Majesty's Stationery Office, 1989.
[23] W. Semar, W. Pannhorst, T.M. Hare, H. Palmour III, Sintering of a crystalline cordierite/ZrO_2 composite, Glastech. Ber. 62 (2) (1989) 74–78.
[24] L.J. Korb, C.A. Morant, R.M. Calland, C.S. Thatcher, The shuttle orbiter thermal protection system, Ceram. Bull. 60 (11) (1981) 1188–1193.
[25] M. Genevrier, A. Mocellin, Reaction sintering and mechanical behavior of cordierite containing sapphirine dispersoids, J. Am. Ceram. Soc. 79 (8) (1996) 2098–2104.
[26] D. Mercurio, P. Thomas, J.P. Mercurio, B. Frit, Y.H. Kim, G. Roult, Powder neutron diffraction study of the thermal expansion of a K-substituted cordierite, J. Mater. Sci. 24 (11) (1989) 3976–3983.
[27] I.M. Lachman, R.D. Bagley, R.M. Lewis, Thermal expansion of extruded cordierite ceramics, Ceram. Bull. 60 (2) (1981) 202–205.
[28] D.L. Evans, G.R. Fisher, J.E. Geiger, F.W. Martin, Thermal expansions and chemical modifications of cordierite, J. Am. Ceram. Soc. 63 (11–12) (1980) 629–634.
[29] H. Ikawa, T. Otagiri, O. Imai, M. Suzuki, K. Urabe, S. Udagawa, Crystal structures and mechanism of thermal expansion of high cordierite and its solid solutions, J. Am. Ceram. Soc. 69 (6) (1986) 492–498.
[30] S.S. Vepa, A.M. Umarji, Effect of substitution of Ca on thermal expansion of cordierite ($Mg_2Al_4Si_5O_{18}$), J. Am. Ceram. Soc. 76 (7) (1993) 1873–1876.
[31] M. Awano, H. Takagi, Synthesis of cordierite and cordierite–$ZrSiO_4$ composite by colloidal processing, J. Mater. Sci. 29 (1994) 412–418.
[32] B.H. Mussler, M.W. Shafer, Preparation and properties of mullite–cordierite composites, Ceram. Bull. 63 (5) (1984) 705–710, 714.
[33] J. Ranachowski, P. Ranachowski, M. Ciesla, G. Zielonka, Modern arc-resistant materials for welding technology, Ind. Ceram. 19 (2) (1999) 103–106.